Desalination and Water Treatment
www.deswater.com

doi: 10.5004/dwt.2017.11423

58 (2017) 351–359
January

Research perspective of membrane distillation: multi-scale and multi-physics phenomena

Albert S. Kim[a,*], Seo Jin Ki[b], Hyeon-Ju Kim[c]

[a]*Department of Civil and Environmental Engineering, University of Hawaii at Manoa, Hawaii 96822, USA, Tel. +1 808 9563718; Fax: +1 808 9565014; email: albertsk@hawaii.edu*
[b]*School of Environmental Science and Engineering, Gwangju Institute of Science and Technology, Gwangju 61005, Korea*
[c]*Seawater Utilization Plant Research Center, Korea Research Institute of Ships & Ocean Engineering, Goseong-gun, Gangwon-do 24747, Korea*

Received 23 December 2015; Accepted 9 May 2016

ABSTRACT

This paper introduces an overview of the principles and discusses current stages and future directions of theoretical and simulation research on membrane distillation (MD). MD as an absolutely two-interface phenomenon consists of microscopic molecular motion, mesoscopic transport, and macroscopic fluid flow. Momentum, heat, and/or mass transfer are dominant in feed, membrane, and distillate regions. We discuss critical issues of MD in various aspects, as follows. Fundamental flaws of using one interface (theoretically induced) are discussed in depth. A general theoretical approach is proposed in terms of a general flux equation developed from statistical physics, and distillate flux is mathematically redefined for hollow fiber MD. Simulation tricks to compare the performances of various membranes and operating conditions are proposed using open source package of OpenFOAM. Big data analysis using a self-organizing map provides specific information regarding key operational parameters for efficient, optimal control of MD plants.

Keywords: Membrane distillation; Multi-scale; Multi-physics; Self-organizing map; OpenFOAM

1. Introduction

Membrane distillation (MD) is a non-isothermal process, in which the driving force is the partial pressure gradient of water vapor along membrane pores [1]. During MD processes, momentum, heat, and mass transfer phenomena occur simultaneously, and their dominances change with respect to various scales of length, time, and material characteristics [2,3]. MD can be categorized into direct contact, sweep gas, vacuum, and air gap MD units, which use different methods to maintain the thermal driving forces for water evaporation and condensation [1]. Fundamental phenomena of MD include: (1) evaporation of water molecules by breaking hydrogen bonds, (2) collective Brownian and Knudsen diffusion through interstitial pore spaces, and (3) condensation in distillate streams [4]. In this work, specific characteristics of MD are discussed in terms of operating conditions and material properties, and multi-scale simulation methods are introduced from molecular to continuum levels [5]. MD is truly sophisticated phenomena because mass, heat, and momentum transport are strongly correlated with each other in feed, membrane, and distillate regions across the hydrophobic porous membrane [6,7]. A rigorous fundamental framework is of great necessity to have a holistic understanding of MD phenomena in terms of the three transport mechanisms, their dominances, and inter-correlations [4,8]. The current work, as a meta-research paper, introduces key issues of MD, discusses thermodynamic fundamentals of transport phenomena, and suggests modeling strategies.

* Corresponding author.

Presented at the 2015 International Environmental Engineering Conference (IEEC 2015) October 28–30, 2015, Busan, Korea.

2. Membrane distillation

2.1. Operation types

MD typically has four types, which are direct contact membrane distillation (DCMD), sweep gas membrane distillation (SGMD), vacuum membrane distillation (VMD), and air gap membrane distillation (AGMD), as shown in Fig. 1. Specific characteristics of various MD processes are briefly summarized in Table 1.

Hot feed of solute concentration is common to all the MD types. Water evaporates at the interface between the hot feed stream and porous membrane surface. In DCMD, a cold (liquid) stream is introduced to the distillate channel to condense the evaporated water molecules coming out of the membrane pores and carry them downstream from the membrane-distillate interface. For dynamic thermal equilibrium in the membrane pores, water evaporates at the feed-membrane interface as fast as water condenses at the membrane-distillate interface. Therefore, the evaporation rate is equal to the condensation rate and should be controlled by the distillate temperature and velocity. The vapor flux primarily depends on temperatures of the hot feed and cold distillate, individually. DCMD is the most applied MD configuration for desalination of seawater and brackish waters, because the condensation unit is well integrated inside the module so that no external condensers are required. Application of DCMD can be conceptually categorized into two cases: removal of toxic components such as boron and arsenic in desalination, and concentration of (valuable) chemical species such as protein solutions in the pharmaceutical industry, acidic solutions in the chemical industry, and fruit juice and milk in the food industry.

SGMD uses a gas flow as the distillate stream, typically air of ambient temperature, to sweep the water vapor downstream from the membrane-distillate interface. Because vapor molecules are swept rapidly, the mass transfer resistance across the membrane is less than that of DCMD, and therefore, SGMD usually provides higher flux than that of DCMD. External condensers are required to collect the water vapor in the distillate stream, which makes the system design complicated with higher cost. SGMD uses a gas as a distillate medium, which has at least one order of magnitude less thermal conductivity than water. The transmembrane heat loss in SGMD is much less than that of DCMD. SGMD is superior to DCMD in removal of volatile organic compounds because SGMD (and VDM as well) is free from wetting risk. Even if such wetting happens inside a SGMD module, transmitted water from the membrane can be collected and drained when needed. SGMD provides about 50% increase in the distillate flux over that of DCMD [9], and incorporating the cold wall of AGMD in SGMD can maintain a low temperature of the sweeping gas, which may enhance the distillate flux.

Table 1
Specific features of different types of MD processes

Types of MD	Feed	Distillate	Phase	Advantages
DCMD	Hot water	Cold water	Liquid	Feasible
SGMD	Hot water	Sweeping air	@ ~1 atm	Higher flux
VMD	Hot water	Vacuum	@ 0.03–1 atm	Highest flux
AGMD	Hot water	Cold surface	Solid	Low cost and flux

The distillate phase of VMD is a low-quality vacuum, that is, a few percent of atmospheric pressure (1 atm). The vacuum pressure in the distillate side should be (much) lower than the vapor pressure evaluated at the hot feed temperature. In the distillate side, the gas density in VMD is much lower than that of SGMD. Based on these two facts, the distillate flux of VMD is usually higher than those of DCMD and SGMD if operating conditions are similar. The transmembrane heat loss is much less than those of DCMD and SGMD because the thermal conductivity of the vacuum phase used in VMD is at least one and two orders of magnitude lower than those of humid air and liquid water, respectively. VMD can be applied for extraction of volatile organic compounds (similar to SGMD), treatment of dilute alcohol water solutions and textile wastewaters, desalination of seawater and brackish waters, concentration of fruit juice, and recovery of aroma compounds.

Vapor molecules passing through the membrane pores contact cold walls and form dew on the cold surfaces in AGMD. For thermodynamic equilibrium, water evaporates at the feed-membrane interface equal to the amount of vapor that forms dew on the cold wall. Humid air fills the space between the distillate side of the membrane and

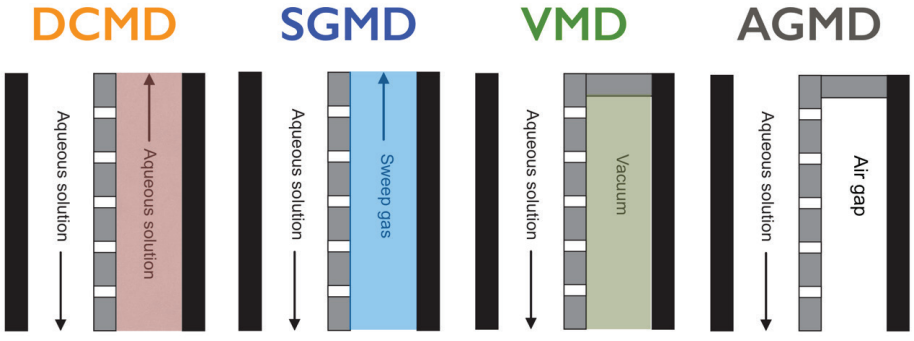

Fig. 1. Schematic illustration of different types of MD.

the cold surface. The transmembrane heat loss is low due to the presence of the humid air in the gap region, but this stationary air gap provides high mass transfer resistance to the migration of water vapor. AGMD has the lowest flux due to high mass transfer resistance, but preparation and maintenance of the cold wall is inexpensive. Potential applications of AGMD in the future seem to be promising due to its low cost and the advantage that it can be combined with SGMD.

2.2. Scale analysis

2.2.1. Length and velocity

In general, MD processes include multiple geometrical scales, as summarized in Table 2. Typical lengths of flat sheet or hollow fiber MD membranes range from 20 to 50 cm, that is, of the order of $O(10^{-1})$ m. A recent study found a critical membrane length existed, above which some membrane area was not fully utilized because the transmembrane temperature gradient became locally zero [10]. Channel height of the flat sheet MD module is about a few millimeters, and the gap between hollow fiber membranes is as much as their outer diameters plus more or less 1 mm. Therefore, the inter-spacing between the MD membrane surfaces is roughly of the order of $O(10^{-3}–10^{-2})$ m. Pore diameters are typically smaller than 1 μm to avoid wetting potential [11]. Although the distillate flux is linearly proportional to the pore size, the liquid entry pressure (LEP) is inversely proportional to the biggest pore sizes. Because the surface porosity of the membrane does not depend on the pore sizes, an optimal pore size can be found, simultaneously toward higher flux and low wetting potential. A membrane having a wide distribution of pore sizes should be avoided in practice. This is because a number of small pores significantly decrease the average flux and larger pores may promote membrane wetting [12]. The pore sizes are of the order of $O(10^{-7}–10^{-6})$ m. Finally, the hydrogen bond length of a water molecule is 0.0958 ≈ 0.1 nm, which is of the order of $O(10^{-10})$ m. The size ratio of the pore size to water molecule size is of the order of $O(10^{3})$, which is strongly related to the mean free path of water vapor. The ratio of the fiber length to pore size is $O(10^{6})$, which controls momentum and mass transfer phenomena. Due to the narrow channel spaces in the flat sheet modules and small gap between fibers, the hot feed and cold distillate (of DCMD) speeds cannot be fast, and they are of the order of $O(10^{-1}–10^{0})$ m/s. The distillate flux of MD is typically of the same order of reverse osmosis $O(10^{-6})$ or less. The ratio of these two velocity scales is about $O(10^{6})$, which is almost equal to the ratio of the fiber length to pore size.

Table 2
Length scales in MD processes

Objects	Length orders	In meters
Hollow fiber length (L_{fiber})	20–50 cm	$O(10^{-1})$
Inter-spacing (h)	1–10 mm	$O(10^{-3}–10^{-2})$
Fiber dimension ($d_o > d_i > d_m$)	~1 mm	$O(10^{-4}–10^{-3})$
Pore diameter (d_{pore})	≤1 μm	$O(10^{-7}–10^{-6})$
Water molecule (H_2O)	~0.1 mm	$O(10^{-10})$

2.2.2. Material properties

Table 3 shows the orders of magnitude of the thermal conductivities for materials used in MD. The thermal conductivity of typical solids ranges from $O(1)$ to $O(10)$ W/m·K, which is the case of the cold wall in AGMD. High thermal conductivity of the cold wall may enhance the vapor condensation rate if the wall is in touch with a cold heat reservoir. In DCMD, both hot feed and cold distillate streams are water. The thermal conductivity of water varies from 561 mW/m·K at 0°C to 679 mW/m·K at 100 °C, which is about one or a few orders smaller than those of typical solids. As indicated above, the water thermal conductivity increases 21% from the freezing to boiling points. Membrane materials used in MD should be hydrophobic [11,12]. Polymer membranes (solid part only) have less thermal conductivity than that of water. Pore spaces of DCMD, SGMD, and AGMD are filled with humid air, that is, a mixture of evaporated water and air molecules. Depending on the humidity, the thermal conductivity of humid air varies from 20 to 30 mW/m·K. Heat transfer across the membrane occurs through the solid part of the membrane, and pore spaces filled with humid air. The thermal conductivity of this solid-gas mixture ranges from 20 to 40 mW/m·K, which is about one order of magnitude smaller than that of the membrane. The membrane porosity is a key factor to determine conductive heat transfer across the membrane [13]. Finally, heat can be transferred through vacuum phases of a low quality, that is, a few percent of the atmospheric pressure. The thermal conductivities increase from vacuum to gas, gas to water, and water to solid. Each increase is of one order. Interestingly, the solid part of the membrane has the thermal conductivities between water and humid air. Specific thermal conductivity values of polyvinylidene fluoride (PVDF), polytetrafluoroethylene (PTFE), and polypropylene (PP) can be found elsewhere [1,8,14].

2.3. Governing equations

When characterized using various physical quantities of different scales, MD turns out to be a truly multi-scale, multi-physics phenomenon dealing with the three standard thermodynamic phases (i.e., gas, liquid, and solid). This

Table 3
Thermal conductivities of materials used in various types of MD

Objects	Distillate phase	κ (mW/m·K])
AGMD	Cold surface (solid)	$O(10^{3}–10^{4})$
DCMD	Water	561–679
	Membrane (solid part only)	100–300
SGMD	Air (humid)	20–30
	Membrane (solid and humid air)	20–40
VMD	Vacuum	4–8

implies that transport phenomena are also subject to the magnitudes of geometrical and physical parameters. To fully investigate the performance of MD processes, governing transport mechanisms need to be identified in feed, membrane, and distillate regions.

2.3.1. Momentum transfer

Momentum transfer is dominant in the hot feed stream of all MD processes. Assuming that the channel flow is in the laminar region, one writes:

$$\frac{1}{\mu}\nabla p = \nabla^2 u \tag{1}$$

where μ is the absolute viscosity of water; p is the hydraulic pressure; and u is the fluid velocity. Note that the water viscosity μ varies from 1.793×10^{-3} Pa·s at the freezing point to 0.2818×10^{-3} Pa·s at the boiling point. The low viscosity of hot feed reduces the pressure gradient to generate a certain feed flow velocity.

2.3.2. Heat transfer

The heat transfer across the membrane consists of conduction through the membrane and convection of vapor carrying the latent heat:

$$Q = -\kappa_{mbr}\nabla T + \overline{H}J_w \tag{2}$$

where κ_{mbr} is the effective thermal conductivity of the mixture of the solid part of the membrane and humid air in the pore spaces, and $\overline{H}$ is the effective enthalpy carried by vapor molecules migrating with the speed of J_w. $\overline{H}$ consists of the latent heat of water and the heat contained by stationary air in the pore spaces.

2.3.3. Mass transfer

In MD, the mass transfer flux is fundamentally equal to the condensation rate per membrane surface. It is often assumed that the vapor flux is proportional to the difference between water vapor pressures at two interfaces [15]:

$$J_w = B_w(p_{v,f} - p_{v,d}) \tag{3}$$

where B_w is the (phenomenological) barometric mass transfer coefficient, and $p_{v,f}$ and $p_{v,d}$ are vapor pressures of water at the feed-membrane and membrane-distillate interfaces, respectively. Because the interfacial vapor pressure is treated as a partial pressure, the barometric diffusion of Eq. (3) can be readily transformed to the conventional Fickian diffusion:

$$J_w = -\frac{\varepsilon}{\tau}D_{\text{eff}}\nabla n \tag{4}$$

where ε and τ are the porosity and tortuosity of the membrane, respectively, and n is the molar concentration of vapor. Here, D_{eff} is the effective diffusivity often estimated using the Bosanquet's relationship [16]:

$$\frac{1}{D_{eff}} = \frac{1}{D_B} + \frac{1}{D_K} \tag{5}$$

where D_B and D_K are Brownian and Knudsen diffusivities, respectively, of which their relative dominance is determined by the mean free path of water molecules. $D_B = D_B(P,T)$ depends on temperature and total pressure of the gas phase. This is because the total pressure P is proportional to the molecular concentration, which determines the inter-molecular collision probability. This inverse relationship between diffusivities is equivalent to resistances in series since the resistance is inversely proportional to the diffusivity. Knudsen diffusivity D_K deals with collisions of individual molecules on microscopically rough pore walls and increases with the mean molecular velocity, proportional to $\sqrt{T}$. Geometry of pore structure plays an important role in Knudsen diffusion.

2.4. Theoretical and simulation methods

2.4.1. Microscopic level of molecular motion

From a fundamental viewpoint, the Bosanquet relationship of Eq. (5) is a proposed relationship between the effective diffusivity and individual diffusivities. An empirical Brownian diffusivity of water vapor [17] is:

$$D_B = \frac{1.895\times10^{-5}}{P[Pa]}T^{2.072} \tag{6}$$

and the fundamental expression of Knudsen diffusivity [18] is:

$$D_K = \frac{1}{3}d_p\sqrt{\frac{8RT}{\pi M_w}} \tag{7}$$

where M_w is the water molecular weight, and d_p is the pore diameter. As discussed above, the relative dominance between D_B and D_K depends on local temperature and the mean free path of water vapor. In reality, vapor molecules in the pore spaces undergo consecutively alternative collisions with vapor/air molecules and local pore walls. Depending on local vapor concentration and pore structures, durations of Brownian and Knudsen diffusion must be not equal. Statistical mechanics simulations such as molecular dynamics and Monte Carlo [19] at large scales should be implemented to accurately estimate diffusion coefficients. These kinds of simulations can provide seamless links between molecular and microscopic continuum levels and avoid the use of empirical and ideal diffusion coefficients. Note that diffusion coefficients are usually dependent on concentrations of diffusing molecules, but both D_B and D_K above are independent of vapor concentration.

2.4.2. Mesoscopic level of transport phenomena

From the viewpoint of fundamental thermodynamics, the vapor flux described by Eqs. (3) and (4) provides only good approximations and needs to be re-investigated, especially for DCMD, SGMD, and AGMD. Without sophisticated investigation, the total pressure in the pore spaces is presumed to 1 atm,

which may be a good, macroscopic approximation, but is not microscopically accurate. For further discussion and simplicity, we neglect the temperature polarization in the membrane interfaces. At the feed-membrane interface inside the pore, the temperature is assumed to be equal to the feed temperature T_f, and the partial pressure of water is assumed to be equal to the water vapor pressure at T_f, that is, $p_v(T_f)$. On the other interface, the distillate temperature is T_d and the water partial pressure is equal to $p_v(T_d)$. Within the pore space, the ideal gas law is assumed to be valid. In this case, the molar concentration of water vapor at the two interfaces (within the pore) are $n_f = p_v(T_f)/RT_f$ and $n_d = p_v(T_d)/RT_d$. The water vapor pressure p_v is highly non-linear with respect to the temperature and so is the molar concentration n. In this case, the partial pressure difference in Eq. (3) does not accurately describe the molecular diffusion because the temperature also varies across the membrane, often monotonously. Here, we need a general representation of the diffusion equation. It should not be thought that J_w depends only on the concentration gradient (or equivalently the partial pressure gradient). The diffusive flux can be written as follows:

$$J_w = -\alpha\nabla\mu - \beta\nabla T \tag{8}$$

where α and β are the coefficients, and μ is the properly defined chemical potential of water vapor. Assuming $\mu = \mu(c, T, P)$, one writes:

$$\mu = \left(\frac{\partial\mu}{\partial c}\right)_{T,P}\nabla c + \left(\frac{\partial\mu}{\partial T}\right)_{c,P}\nabla T + \left(\frac{\partial\mu}{\partial P}\right)_{c,T}\nabla P \tag{9}$$

where $\partial_x\mu = \partial\mu/\partial x$ ($x = c, T, P$), and P is the total pressure, that is, a sum of partial pressures of water and air molecules in the pore spaces. Substitution of Eq. (9) into Eq. (8) gives:

$$J_w = -\alpha\left(\frac{\partial\mu}{\partial c}\right)_{T,P}\nabla c - \left[\alpha\left(\frac{\partial\mu}{\partial T}\right)_{c,P} + \beta\right]\nabla T - \alpha\left(\frac{\partial\mu}{\partial P}\right)_{c,T}\nabla P \tag{10}$$

of which the first, second, and third terms on the right side are Fickian diffusion, thermal diffusion, and baro-diffusion, respectively. Eq. (10) indicates several important issues in modeling vapor diffusion through the MD membrane pores. The first term is equivalent to Eq. (3) or (4), which implies the chemical potential μ includes all the possible diffusion mechanisms of water vapor including Brownian and Knudsen diffusion, as functions of temperature T and total pressure P. The second term indicates that the temperature-induced diffusion has two contributions: one is from the dependence of the chemical potential on T, and the other is thermal conduction. In a closed space, the temperature of an ideal gas is related to the kinetic energy of gas molecules:

$$\frac{1}{2}mv^2 = \frac{1}{2}K_BT \tag{11}$$

where K_B is the Boltzmann constant. The temperature gradient implies spatial changes in the molecular kinetic energy and hence the net motion of gas molecules to a lower temperature region. In the same light, the thermal convection is not independent of molecular diffusion. The third term of Eq. (10) is the true baro-diffusion, which is often replaced by or referred to as viscous flow or Hagen-Poiseuille flow. The baro-diffusion is important in VDM and SGMD because the pore spaces are not closed like DCDM and AGMD. The true difficulty in MD modeling shows the strong coupling of mass transfer Eq. (10) with heat transfer Eq. (2) [4,8].

2.4.2.1. Accurate governing equation

In continuum theoretical approaches, some fundamental flaws are recently re-addressed. First, the effect of membrane thickness is often disregarded so that the governing equation of a differential form is approximated as that of difference form. The vapor flux Eq. (3) should be written in terms of the pressure gradient instead of the pressure difference. In addition, the partial pressures of water vapor at the interior interfaces are very hard to measure so that Eq. (3) is written as follows:

$$J_w = C_m\frac{dp_v}{dT}\left[T_f - T_d\right] \tag{12}$$

where dp_v/dT represents the variation of the water vapor pressure with respect to temperature. Note that C_m and dp_v/dT are functions of temperature. The temperature difference between T_f and T_d as well as $C_m(dp_v/dT)$ should be evaluated at a certain temperature within the membrane thickness δ_m. The mean temperature $\overline{T} = (T_f + T_d)/2$ is often used as an optimal choice by rule of thumb [20], which can be acceptable only if the temperature difference is not big. This approach implicitly treats a membrane as a porous sheet of zero thickness, having only one mathematical interface. Some flawed results are discussed in our recent work [2]. If the pore is assumed to be straight, then the vapor flux J_w is constant along the pore. Eq. (12) should be written in terms of two independent variables, the position along the pore x and the temperature as a function of x, and these variables are separated to integrate each side of Eq. (12). Conversely, evaporation and condensation at two interfaces should be individually taken into account.

2.4.2.2. Mass/heat fluxes across hollow fiber membranes

Membrane performance is evaluated by the flux, conceptually defined as follows:

$$J_w = \frac{\text{Distillate flow rate(Collected water volume/Time)}}{\text{Membrance surface area}} \tag{13}$$

The surface area of hollow fiber membrane is $A_m = 2\pi DL$, where L is the fiber length, and D is the inner or outer diameters. Which diameter is used to calculate the flux? Here, the distillate flux should be redefined to accurately compare the performances of membranes and/or operating conditions. In the steady state ($\partial/\partial t = 0$), the vapor flux should satisfy the following condition:

$$\nabla \cdot J_w = 0 \tag{14}$$

because water molecules are neither created nor annihilated. Variations of J_w in the axial and azimuthal directions are negligible so that:

$$\frac{1}{r}\frac{\partial}{\partial r}(rJ_r) = 0 \tag{15}$$

where $J_r(\approx J_w)$ is the (dominant) radial component of J_w. Eq. (15) clearly indicates that rJ_r is constant. A new definition of the distillate flux through hollow fiber membranes is suggested:

$$F_w = J_w r = \frac{\text{Condensation rate}}{2\pi L} \tag{16}$$

which is interpreted as condensed mass of water vapor per unit time and unit fiber length. The heat flux should have a similar definition:

$$S_q = q_r r = \frac{\text{Heat transfer rate}}{2\pi L} \tag{17}$$

where q_r is the radian component of the conventional heat flux q, corresponding to J_w.

2.4.3. Macroscopic level of fluid mechanics

Recent academic attention to MD processes requires more rigorous investigation using multi-scale simulations, which are able to simultaneously simulate complex fluid flow with mass or heat transfer. Open Field Operation and Manipulation (OpenFOAM) is an open source computational fluid dynamics software package, having extensive ranges of features to solve (coupled) mass, momentum, and heat transfer phenomena. Among many solvers included in OpenFOAM (OF), *chtMultiRegionFoam* solves coupled momentum and heat transfer phenomena [21]. OF simulation has three steps. First, geometrical information of the space in which fluid flows needs to be specified. The geometry of the entire fluid body should be defined by a 3-dimensional (3D) mesh because OF does not have (pure) 2-dimensional (2D) solvers. The embedded tool for mesh generation in OF is *BlockMesh*. To use it, users should generate a script file, called BlockMeshDict. Unless the geometry of the fluid body is simple such as a pipe and rectangular duct, the use of *BlockMesh* is generally discouraged. In addition to a number of commercial meshing programs, GMSH and NETGEN are open source programs, which can be used to solve engineering problems with moderate geometrical complexities [22]. Once a mesh is ready with specific boundary names, boundary conditions for the fluid velocity *U* and the pressure *p* need to be specified in files of the same names. Depending on solvers, there are more initial files in addition to *U* and *p*. Running a OF solver can be performed in two modes: serial and parallel. Users can only define the method of domain decomposition and how to split the computational domain in *x*, *y*, and *z* directions. After completing a simulation run, numerical results can be visualized using scientific visualization software. One of the most widely used programs is ParaView, often integrated in OF as a similar name, *paraFoam* [23].

Although the application potential of OF to engineering discipline looks almost limitless, no specific solver is yet available to investigate strongly coupled phenomena of mass/momentum/heat transfer across the MD membranes. Because OF is an open-source software, advanced users can develop their own solvers by changing or modifying source codes of existing solvers written in C++. But, this process is usually challenging. Here, we introduce a conceptual method that allows estimating the convective heat flux, which is the heat carried by the migrating vapor per unit time and cross-sectional surface. As indicated above, the transmembrane vapor flux is about $O(10^6)$ times smaller than the channel velocity in the MD module. In this case, it is numerically difficult to calculate how many vapor molecules entered into and left in the membrane per unit time. The magnitude of this vapor flux must be within a tolerance error of the channel velocity.

In DCMD and AGMD, the baro-diffusion, the third term in the right side of Eq. (10), is negligible. Using the ideal gas law, the vapor concentration c can be represented in terms of temperature T. Then, the heat flux Eq. (2) can be simply rewritten as follows:

$$Q_{\text{total}} = Q_{\text{mbr}} + Q_{\text{vapor}} \tag{18}$$

$$Q_{\text{mbr}} = -K_{\text{mbr}}\nabla T \tag{19}$$

$$Q_{\text{vapor}} = -K_{\text{vapor}}\nabla T \tag{20}$$

where Q_{mbr} is the conductive heat transfer rate though the mixture of the solid part of the membrane and humid air in the pore spaces. We calculate the effective thermal conductivity κ_{mbr} as a function of $\kappa_s(T)$ of the solid membrane part, $\kappa_g(T)$ of the humid air, and the membrane porosity ε. We can do OF simulation twice with $Q = Q_{\text{totol}}$ and $Q = Q_{\text{mbr}}$. Note that κ_{mbr} includes the effect of thermal conduction due to the solid membrane part and stationary mixture of vapor and air molecules in the interstitial pore spaces, and κ_{vapor} is due to migration of the humid gas in the pore. Cancelling κ_{vapor} term in heat transfer is equivalent to the condition that allows the presence of humid air in the pore spaces, but blocks their migration by closing pore inlets and outlets using an imaginary layer of zero thickness and infinite thermal conductivity. By integrating the heat flow rate at the membrane-distillate interface, the heat fluxes with and without Q_{vapor} can be calculated, and their difference indicates the convective heat flux carried by the migrating vapor molecules. Due to the non-linearity of κ, taking the difference must be a better approximation than using $Q = Q_{\text{vapor}}$. We can calculate the mean vapor flux using the calculated heat flux difference:

$$\langle J_w \rangle = \frac{\langle Q_{\text{total}} \rangle - \langle Q_{\text{mbr}} \rangle}{\left\langle \bar{H} \right\rangle} \tag{21}$$

where the brackets ⟨ ⟩ indicate the integrated average over the membrane-distillate interface. The magnitude of J_w provides only an approximate value of the measurable distillate flux across the flat sheet membrane, but it can be rigorously used to compare the performances of a single membrane under various operating conditions or different membranes under a given operating condition. Details of this MD simulation technique using OF will be found in our future publications.

2.4.4. Statistical level of big data analysis

Dynamic simulation of MD membranes under various operating conditions generates immense quantities of data which are difficult to interpret readily with simple statistical methods [24]. For instance, if there are 8 operating parameters to which we assign 7 different values, candidate sets of parameter values for simulation of MD membranes exceed 5 million cases (7^8 = 5,764,801). Output files quickly reach a size in excess of several terabytes which require specific handling of reducing the file size so that only a single value for the parameter of interest is returned and then compiled for subsequent statistical analyses. As discussed in the previous sections, simulation of MD membranes spans 9 orders of magnitude in both length scale and physical process (Fig. 2). The relationship either between the dependent (or output) and independent (or input) parameters or between themselves may not be linear depending on the level of physical processes as well as at the given process level. This makes use of more sophisticated statistical tools that can properly align multi-scale parameters and multi-physics behavior of MD processes by rigorously handling dependencies among parameters (i.e., multicollinearity issue). A non-linear data analysis typically outperforms a linear method when relationships between parameters are highly non-linear for the full range of operations [25,26]. The entire data set used for statistical analyses may consist of real and dimensionless parameters examined and derived from all possible operating conditions.

2.4.4.1. Self-organizing map

Self-organizing map (SOM), developed by Teuvo Kohonen in the 1980s, is a popular tool, which uses topology preservation and vector quantification algorithms to effectively reduce the data dimensionality while retaining information in the original, high-dimensional data set [27]. The variation in the data set can be well captured with a reduced number of data samples (or prototype vectors) that are systematically visualized in a low-dimensional grid space (e.g., 2D or 3D). As an unsupervised neural network, SOM provides a robust analysis in characterizing non-linear data patterns such as unknown clusters and relationships between parameters. In addition, it efficiently removes noise and outliers from the data set during the training process which is performed by initialization and training algorithms. SOM toolbox, an implementable package for MATLAB 5, is freely available online (at http://www.cis.hut.fi/somtoolbox/), and detailed information on theory and its applications are fully documented elsewhere [24,27,28].

2.4.4.2. Multiple linear regression

Multiple linear regression (MLR) is an approach for addressing the relationship between a dependent and multiple independent parameters in a linear fashion. Accuracy in MLR will be improved when parameters in the data set follow parametric assumptions (e.g., normality and linearity) well and are free of the multicollinearity issue. Because of its convenience in terms of formula and computation, many researchers rely on MLR or its variants to compare and display their prediction and actual output values [29]. MLR can be performed with standard statistical software such as SAS, SPSS, or even MATLAB through Statistics Toolbox [30].

Our previous study [24] shows an example of big data analysis conducted for the data set that is created from a large simulation of hollow fiber direct contact membrane distillation (HFDCMD) using software, hfdcmd, developed under Environmental Physics Software. More than 10 million simulations were done for estimating two (output) parameters, mass (for $\langle F_w \rangle$) and heat transfer rates per fiber length (for $\langle S_q \rangle$), and around 7.5 million cases of these were selected for further statistical analyses. SOM and MLR were used to analyze two large data sets: a physical data set consisting of 12 input and 2 output parameters, and dimensionless data set including 10 input and 2 output numbers. The dimensionless data set is prepared using the original (physical) data set. Note that two dimensionless numbers which are equivalent to real output parameters $\langle F_w \rangle$ and $\langle S_q \rangle$ are $\mathrm{Pe}_{\mathrm{mbr}}$ (i.e., Peclet_mbr) and $\mathrm{Nu}_{\mathrm{mbr}}$ (i.e., Nusselt_mbr), respectively. Fig. 2 shows links between process levels at certain length scales and how they are incorporated in SOM and MLR analyses.

From the results of statistical analyses [24], SOM successfully captured the relationship among 14 physical parameters through nonlinear mapping of spatial patterns in hexagonal grid (namely component planes). However, no clear relationship was found between the two outputs and any of the remaining inputs, reflecting the complexity of multi-physics phenomena in HFDCMD in terms of strongly correlated mass, heat, and momentum transfer phenomena. Six clusters determined by the similarity of the physical parameters well characterized the entire data set. Interestingly, more homogenous data patterns were

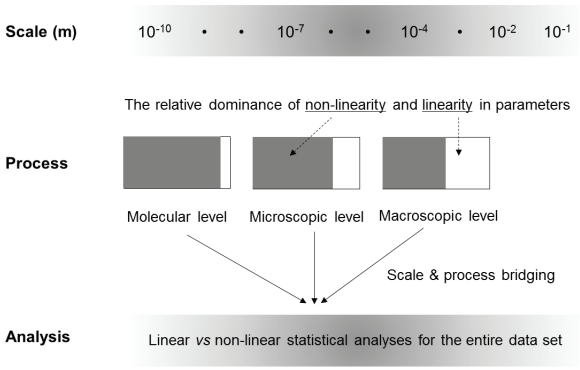

Fig. 2. A conceptual diagram encountered for statistical analyses of a large data set obtained from multi-scale and multi-physics simulations of MD.

found in the dimensionless data set, but prediction of the MD performance was still not straightforward. In contrast, MLR directly assessed the performance of HFDCMD using only 3–4 key input parameters regardless of the types of data sets that included either only physical or dimensionless parameters. Macroscopic quantities (e.g., temperature and radii in the feed and permeate streams) played a much more important role in controlling the HFDCMD performance than microscopic quantities that were several orders of magnitude smaller than macroscopic parameters. Overall, these results demonstrated that advanced data analysis tools helped address the complex characteristics of the performance in HFDCMD, but only partially explained the driving force of transfer phenomena due to the intrinsic coupling of MD processes.

3. Concluding remarks

We discussed the fundamental characteristics of MD processes in multi-scale and multi-physics viewpoints. From microscopic water evaporation and macroscopic fresh-water production, the length scales, mass fluxes, and heat fluxes have multiple of orders of $O(10^9)$, $O(10^6)$, and $O(10^3)$, respectively. The strong coupling of two transfer phenomena in lumen and shell regions makes a holistic understanding of MD processes difficult and rigorous prediction more challenging. Evaporation and condensation are individual sub-processes occurring at two interfaces across the membrane so that mathematical approximation should not violate the physical situations by considering a single interface for phase change. In hollow fiber MD processes, distillate flow rate of heat and mass needs to be divided by the fiber length (rather than the membrane surface area) so that the new flux definition is distillate flow rate (of heat and mass) per unit hollow fiber membrane length. In hollow fiber MD, the hot feed should flow in the lumen and shell channels, depending on the availability of heat source. The condensation rate will be then limited by the temperature and speed of the cold distillate stream. Analyzing big data of MD simulations implies the complexity and inter-dependence of physical quantities of MD, which allows us to sort out three to four important controlling parameters. The advanced statistical tools, such as SOM and MLR, help us optimize MD processes by controlling the selected key parameters of different scales. Identifying the dominant transfer phenomena in each length-scale and seamlessly linking them across the membrane interfaces will provide a holistic understanding of the inter-convoluted phenomena and a better performance optimization.

Acknowledgment

This work was financially supported by the National R&D project of "Development of new application technology for deep seawater industry" funded by the Ministry of Oceans and Fisheries of the Republic of Korea.

References

[1] P. Wang, T.S. Chung, Recent advances in membrane distillation processes: membrane development, configuration design and application exploring, J. Membr. Sci., 474 (2015) 39–56.
[2] M. Mulder, Basic principles of membrane technology, Kluwer Academic Publishers, Boston, 1996.
[3] M. Khayet, T. Matsuura, Membrane distillation: principles and applications, Elsevier, New York, 2011.
[4] Ó. Andrjesdóttir, C.L. Ong, M. Nabavi, S. Paredes, A.S.G. Khalil, B. Michel, D. Poulikakos, An experimentally optimized model for heat and mass transfer in direct contact membrane distillation, Int. J. Heat Mass Transfer, 66 (2013) 855–867.
[5] E. Curcio, E. Drioli, Membrane distillation and related operations—a review, Sep. Purif. Rev., 34 (2005) 35–86.
[6] M. Khayet, Membranes and theoretical modeling of membrane distillation: a review, Adv. Colloid Interface Sci., 164 (2011) 56–88.
[7] A. Alkhudhiri, N. Darwish, N. Hilal, Membrane distillation: a comprehensive review, Desalination, 287 (2012) 2–18.
[8] I. Hitsov, T. Maere, K. De Sitter, C. Dotremont, I. Nopens, Modelling approaches in membrane distillation: a critical review, Sep. Purif. Technol., 142 (2015) 48–64.
[9] M. Khayet, M.P. Godino, J.I. Mengual, Possibility of nuclear desalination through various membrane distillation configurations: a comparative study, Int. J. Nucl. Desal., 1 (2003) 30–46.
[10] A.S. Kim, Cylindrical cell model for direct contact membrane distillation (DCMD) of densely packed hollow fibers, J. Membr. Sci., 455 (2014) 168–186.
[11] P. Wang, T.S. Chung, Design and fabrication of lotus-root-like multi-bore hollow fiber membrane for direct contact membrane distillation, J. Membr. Sci., 421–422 (2012) 361–374.
[12] P. Wang, T.S. Chung, A new-generation asymmetric multi-bore hollow fiber membrane for sustainable water production via vacuum membrane distillation, Environ. Sci. Technol., 47 (2013) 6272–6278.
[13] N.N. Li, A.G. Fane, W.S.W. Ho, T. Matsuura, Advanced membrane technology and applications, John Wiley & Sons, New Jersey, 2011.
[14] A.S. Kim, A two-interface transport model with pore-size distribution for predicting the performance of direct contact membrane distillation (DCMD), J. Membr. Sci., 428 (2013) 410–424.
[15] G. Zuo, G. Guan, R. Wang, Numerical modeling and optimization of vacuum membrane distillation module for low-cost water production, Desalination, 339 (2014) 1–9.
[16] C.H. Bosanquet, The optimum pressure for a diffusion separation plant, British TA Report, BR/507 (1944).
[17] T.R. Marrero, E.A. Mason, Gaseous diffusion coefficients, J. Phys. Chem. Ref. Data, 1 (1972) 3–118.
[18] M. Knudsen, W.J. Fisher, The molecular and the frictional flow of gases in tubes, Phys. Rev. (Series I), 31 (1910) 586–588.
[19] Y. Shi, Y. Lee, A. Kim, Knudsen diffusion through cylindrical tubes of varying radii: theory and Monte Carlo simulations, Transport Porous Med., 93 (2012) 517–541.
[20] E. Drioli, A. Ali, F. Macedonio, Membrane distillation: recent developments and perspectives, Desalination, 356 (2015) 56–84.
[21] J.L.C. Santos, V. Geraldes, S. Velizarov, J.G. Crespo, Investigation of flow patterns and mass transfer in membrane module channels filled with flow-aligned spacers using computational fluid dynamics (CFD), J. Membr. Sci., 305 (2007) 103–117.
[22] J. Storm, M. Abendroth, M. Emmel, T. Liedke, U. Ballaschk, C. Voigt, T. Sieber, M. Kuna, Geometrical modelling of foam structures using implicit functions, Int. J. Solids Struct., 50 (2013) 548–555.
[23] B. Prasad, T. Hino, K. Suzuki, Numerical simulation of free surface flows around shallowly submerged hydrofoil by OpenFOAM, Ocean Eng., 102 (2015) 87–94.
[24] S.J. Ki, H.-J. Kim, A.S. Kim, Big data analysis of hollow fiber direct contact membrane distillation (HFDCMD) for simulation-based empirical analysis, Desalination, 355 (2015) 56–67.
[25] A. Akhbardeh, M.A. Jacobs, Comparative analysis of nonlinear dimensionality reduction techniques for breast MRI segmentation, Med. Phys., 39 (2012) 2275–2289.
[26] J.W. Hall, S.A. Boyce, Y. Wang, R.J. Dawson, S. Tarantola, A. Saltelli, Sensitivity analysis for hydraulic models, J. Hydraul. Eng.-ASCE, 135 (2009) 959–969.

[27] J. Vesanto, J. Himberg, E. Alhoniemi, J. Parhankangas, SOM Toolbox for MATLAB 5, Report A57, SOM Toolbox Team, Helsinki University of Technology, Espoo (2000).
[28] S.J. Ki, J.-H. Kang, S.W. Lee, Y.S. Lee, K.H. Cho, K.-G. An, J.H. Kim, Advancing assessment and design of stormwater monitoring programs using a self-organizing map: characterization of trace metal concentration profiles in stormwater runoff, Water Res., 45 (2011) 4183–4197.
[29] F. Pianosi, K. Beven, J. Freer, J.W. Hall, J. Rougier, D.B. Stephenson, T. Wagener, Sensitivity analysis of environmental models: a systematic review with practical workflow, Environ. Model. Softw., 79 (2016) 214–232.
[30] A. Field, Discovering statistics using SPSS, 2nd ed., SAGE Publications, Thousand Oaks, 2005.